



HAL
open science

Phase diagrams of Kondo alloys

Bishal Poudel, Gertrud Zwicknagl, Claudine Lacroix, Sébastien Burdin

► **To cite this version:**

Bishal Poudel, Gertrud Zwicknagl, Claudine Lacroix, Sébastien Burdin. Phase diagrams of Kondo alloys. *Journal of Magnetism and Magnetic Materials*, 2021, 520 (167405), 10.1016/j.jmmm.2020.167405 . hal-03109515

HAL Id: hal-03109515

<https://hal.science/hal-03109515>

Submitted on 13 Jan 2021

HAL is a multi-disciplinary open access archive for the deposit and dissemination of scientific research documents, whether they are published or not. The documents may come from teaching and research institutions in France or abroad, or from public or private research centers.

L'archive ouverte pluridisciplinaire **HAL**, est destinée au dépôt et à la diffusion de documents scientifiques de niveau recherche, publiés ou non, émanant des établissements d'enseignement et de recherche français ou étrangers, des laboratoires publics ou privés.

Phase diagrams of Kondo alloys

Bishal Poudel^{a,*}, Gertrud Zwicknagl^b, Claudine Lacroix^c, Sébastien Burdin^a

^a Université Bordeaux, CNRS, LOMA, UMR 5798, 33400 Talence, France

^b Institut für Mathematische Physik, Technische Universität Braunschweig, Mendelssohnstrasse 3, D-38106 Braunschweig, Germany

^c Institut Néel, CNRS et Université Joseph Fourier, BP 166, F-38042 Grenoble Cedex 9, France

A B S T R A C T

We analyze the ground state phase diagrams of the Kondo alloy model (KAM) as a function of Kondo coupling (J_K), electronic band filling (n_c) and magnetic impurity concentration (x). We use DMFT/CPA method to treat the disorder and the inter-site electronic exchange correlations along with mean-field (MF) approximations to decouple the Kondo interaction. Here, we generalize “Doniach-like” phase diagrams of the periodic Kondo lattice ($x = 1$) to Kondo alloys. We consider the competition between the paramagnetic Kondo phase (K) and purely ferromagnetic (F) or staggered antiferromagnetic (AF) ordered phases. Our phase diagrams are consistent with various experimentally obtained phase diagrams for alloys like $\text{Ce}_x\text{La}_{1-x}\text{Pt}_2\text{Si}_2$, $\text{Ce}_x\text{La}_{1-x}\text{Ni}_2\text{Ge}_2$, $\text{Ce}_x\text{La}_{1-x}\text{Ru}_2\text{Si}_2$, $\text{Ce}_x\text{La}_{1-x}\text{Pd}_2\text{Si}_2$, or $\text{Ce}_x\text{La}_{1-x}\text{Cu}_2\text{Ge}_2$.

1. Introduction

The single impurity Kondo effect has been extensively studied [1–4] for decades. It results from a local antiferromagnetic coupling J_K between conduction electrons spins and the spin of quantum magnetic impurities. At low temperature, it is characterized by the formation of local non-magnetic singlets, below the Kondo temperature T_K . Kondo effect was observed in transition metals alloys with low magnetic impurities concentration (as Mn or Fe), and also in rare-earth materials like Ce or Yb based compounds.

In concentrated Kondo systems, various types of ground states can be stabilized giving rise to rich phase diagrams with a large diversity of unconventional quantum phases and behaviors[5]. These include unconventional superconductivity[6,7] as observed, e.g. in CeCu_2Si_2 [8] or non-Fermi liquids behavior [9]. Application of pressure on these systems usually increases the Kondo interaction thus yielding a phase transition from magnetic ordering to a paramagnetic phase. This behavior can be understood by Doniach’s argument [10]: Kondo energy scale $T_K \propto \frac{1}{\rho_0} \exp\left(-1/J_K \rho_0\right)$ competes with the Ruderman-Kittel-Kasuya-

Yoshida state (RKKY) inter-impurity magnetic interaction $J_{\text{RKKY}} \propto J_K^2 \rho_0$. Here, ρ_0 is density of conduction electron states, J_K is Kondo coupling. $\rho_0 J_K$ is affected by pressure: increasing pressure in Ce-based compounds increases $\rho_0 J_K$ and induces a transition from a magnetically ordered phase to paramagnetic Kondo phase, whereas the contrary occurs in Yb-

based materials.

In Kondo systems, another pertinent parameter besides pressure is the electronic filling of the conduction band (n_c). Multiple theoretical studies were conducted in order to explore the effect of n_c for Kondo lattice model (KLM) with varieties of complementary approaches. Lacroix and Cyrot calculated the first Kondo lattice phase diagram [11] by using mean-field approximations, thereafter multiple theoretical techniques [12–14] were used to refine and explore it. All these theoretical studies revealed Doniach-like phase diagrams.

Nozières [15] raised the question of ‘exhaustion’ regarding how a coherent Fermi liquid Kondo ground state can be formed when the concentration of Kondo impurities is larger than the concentration of conduction electrons and he proposed that there are 2 energy scales, the Kondo temperature T_K and a coherence temperature lower than T_K . This proposition was discussed in many papers and authors now agree that the ratio of these 2 energy scales depend only on the band filling n_c [16–20].

On the other hand, the concentration of Kondo impurities x is a parameter that can be finely tuned allowing to study the issue of coherence in Kondo alloys. Multiple experimental studies of Ce-La substitution shows that substitution can give rise to magnetically ordered phase like in $\text{Ce}_x\text{La}_{1-x}\text{Ru}_2\text{Si}_2$ [21], non-Fermi liquid properties like in $\text{Ce}_x\text{La}_{1-x}\text{Ni}_2\text{Ge}_2$ [22], persistence of magnetically ordered phase up to low concentration of Cerium like in $\text{Ce}_x\text{La}_{1-x}\text{Cu}_2\text{Ge}_2$ [23] or simply diminution of T_K without long range magnetic order in $\text{Ce}_x\text{La}_{1-x}\text{Pt}_2\text{Si}_2$

[24].

Meanwhile, theoretical studies conducted in [25] by Dynamical Mean Field Theory (DMFT) which was equivalent to a matrix version of the Coherent Potential Approximation (CPA) and in [26] by CPA shows that T_K doesn't depend on x . Recently in [27] the local potential scattering was studied for the Kondo alloy model (KAM) with stat-DMFT. Here in our work, we will address a theoretical model to understand the stability of magnetic phases in Kondo alloys.

In our work, we extend the matrix DMFT/CPA approach developed by Burdin and Fulde in ([25]) to include the magnetic ordered phases.

In this article, we develop a general formalism to study the effect of substitution on the ground state phase diagram with respect to the parameters J_K (Kondo coupling), n_c (electronic filling) and x (concentration of Kondo impurities) extending Doniach phase diagrams to the Kondo alloys. The formalism developed is very general and can also be used to study other effects like the disorder effects on Fermi surfaces or photoemission spectroscopy. We start this paper by explaining model, methods and approximations in the second section and in the third section, we present the results and in the last section we compare our results with those obtained by Ce-La substitution.

2. Model, methods and approximations

2.1. Kondo alloy model

The Kondo alloy model (KAM) Hamiltonian is written as

$$H = \sum_{ij\sigma} \left(t_{ij} - \mu \right) c_{i\sigma}^\dagger c_{j\sigma} + J_K \sum_{i \in \mathcal{K}} \mathbf{S}_i \mathbf{s}_i + \mu N n_c, \quad (1)$$

where $c_{i\sigma}^{(\dagger)}$ corresponds to annihilation (creation) operators for conduction electrons with i and $\sigma = \uparrow, \downarrow$ respectively site and spin components. $J_K > 0$ is the local Kondo antiferromagnetic interaction between the local spin density of conduction electrons, \mathbf{s}_i , and quantum spin 1/2 operators \mathbf{S}_i representing Kondo impurities. The Kondo impurities are randomly distributed with a concentration x on a sub-part \mathcal{K} of the periodic lattice with N sites. The complementary non-Kondo sites, with concentration $1 - x$, will be denoted \mathcal{N} . The electronic filling $n_c = \frac{1}{N} \sum_{i\sigma} \langle c_{i\sigma}^\dagger c_{i\sigma} \rangle$ per site is fixed by tuning the chemical potential μ . The nearest-neighbor inter-site electronic hopping energy t_{ij} is considered constant, $t_{ij} = t$, irrespectively from the nature \mathcal{K} or \mathcal{N} of sites i and j . Generally in this work, we consider the KAM on the 2D 'square' lattice; However, in the special case of a periodic Kondo lattice ($x = 1$) we have also considered 1D 'chain' and 3D 'cubic' lattices. For the sake of clarity, in the next section we present only the specific DMFT/CPA method that we developed on a square lattice. The adaptation to other cases is straightforward.

2.2. DMFT/CPA method

We took into account the randomness of the \mathcal{K} sites distribution using a DMFT/CPA [28,25] approach. First, the action related with the KAM Hamiltonian Eq. (1) is expressed as

$$S = S^0 - \sum_{ij\sigma} \int_0^\beta d\tau c_{i\sigma}^\dagger(\tau) \left\{ \left(\partial_\tau - \mu \right) \delta_{ij} + t_{ij} \right\} c_{j\sigma}(\tau) - \int_0^\beta d\tau J_K \sum_{i \in \mathcal{K}} \mathbf{S}_i(\tau) \mathbf{s}_i(\tau), \quad (2)$$

where $\beta = 1/T$ is the inverse temperature, τ denotes imaginary time, and $S^0 = -\beta \mu N n_c$. Hereafter, we will be following the formalism developed in [25]. In this previous work only Kondo and non-Kondo paramagnetic solutions were considered. Here, we generalize this technique to take account the possibility of magnetically ordered phases (ferromagnetic or antiferromagnetic with ordering vector $\mathbf{Q} = (\pi, \pi)$).

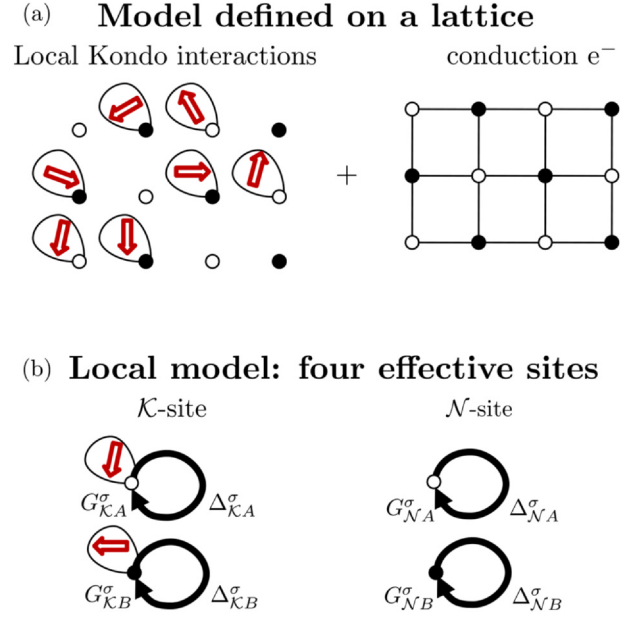


Fig. 1. Schematic view of generalized matrix-DMFT approach of mapping a lattice problem (a) onto four effective sites (b) in a bipartite system interacting with dynamical effective local bath in each case, where \bullet denotes sub-lattice A and \circ denotes sub-lattice B, red arrows are Kondo impurity spins located at random sites and the black arrows denotes the dynamical local baths. (For interpretation of the references to color in this figure legend, the reader is referred to the web version of this article.)

DMFT allows to map a lattice problem to an effective single site problem embedded in a self-consistent dynamical mean field which captures the influence of all neighboring sites [28]. In our approach, we consider a square lattice that is formally split into two sublattices A and B as depicted on Fig. 1. We then apply the DMFT method considering a site α that belongs to a given sub-lattice $\alpha = A$ or B and which is of nature $a = \mathcal{K}$ or \mathcal{N} . As a result, the KAM is mapped onto four effective single site problems embedded with dynamical local baths.

2.2.1. Local actions

Following the standard DMFT approach [28] we rescale the hopping as $t_{ij} = \tilde{t}_{ij}/\sqrt{z}$, where z is related to the coordination number of the lattice. In the following we will assume z is large and thus neglect $1/z$ corrections in diagrammatic expansions. Furthermore, we assume that the local \mathcal{K} or \mathcal{N} configuration of each site is not correlated with the configuration of neighboring sites, hence the dynamical local bath ($\Delta_{\alpha\sigma}$) for \mathcal{K} or \mathcal{N} sites are identical, so $\Delta_{\mathcal{K}A}^\sigma(\tau) = \Delta_{\mathcal{N}A}^\sigma(\tau) = \Delta_{\alpha\sigma}^\sigma(\tau)$. Hence, each effective site is characterized by a local effective action as

$$S_\alpha^\mathcal{K} = - \sum_\sigma \int_0^\beta d\tau \int_0^\beta d\tau' c_{\mathcal{K}\alpha\sigma}^\dagger(\tau) \left(\partial_\tau - \mu \right) \delta_{\tau-\tau'} + \Delta_{\alpha\sigma}(\tau - \tau') c_{\mathcal{K}\alpha\sigma}(\tau') - J_K \int_0^\beta d\tau \mathbf{S}_\alpha(\tau) \mathbf{s}_\alpha(\tau), \quad (3)$$

and

$$S_\alpha^\mathcal{N} = - \sum_\sigma \int_0^\beta d\tau \int_0^\beta d\tau' c_{\mathcal{N}\alpha\sigma}^\dagger(\tau) \left(\partial_\tau - \mu \right) \delta_{\tau-\tau'} + \Delta_{\alpha\sigma}(\tau - \tau') c_{\mathcal{N}\alpha\sigma}(\tau'), \quad (4)$$

where $\alpha = A, B$. Like in usual DMFT formalism [28], the dynamical local bath $\Delta_{\alpha\sigma}(\tau) = \sum_{ij} \tilde{t}_{\alpha i} \tilde{t}_{j\alpha} \left\langle c_{i\sigma}(\tau) c_{j\sigma}^\dagger(\tau') \right\rangle_{(\alpha)}$ can be expressed in terms of the cavity (α, a) electronic Green's functions, that means using the KAM action (2) without the contribution of the local site (α, a). More details on the self-consistent procedure will be published elsewhere.

Table 1

Table that resumes local Green's function invariance according to the transformations for K, F and AF II phases. From the table, sites A and B are equivalent for F and K phases, while in AF phase electrons on sub-lattice A with spin σ are equivalent to electrons on sublattice B with spin $\bar{\sigma}$.

Transformations	Invariance		
	K	F	AF II
A \rightarrow B $\sigma \rightarrow \bar{\sigma}$	yes	no	yes
A \rightarrow B $\sigma \rightarrow \sigma$	yes	yes	no
A \rightarrow A $\sigma \rightarrow \bar{\sigma}$	yes	no	no

2.2.2. Symmetries considerations

In our study of Kondo alloys, we consider only pure paramagnetic Kondo phase (K), pure ferromagnetic phase (F) or antiferromagnetic (AF II) phase with staggered Néel order $\mathbf{Q} = (\pi, \pi)$. The choice of this specific staggered Néel order is very convenient for the DMFT/CPA method which can use the bipartiteness of the lattice. Using the DMFT/CPA method, the lattice problem has been mapped onto four single site effective problems that account for the possible local correlations, $a = N$ or K , on sublattice $\alpha = A$ or B .

In Table 1 we analyse symmetry properties of the various phases that we consider. For different reasons, in each case, the problem can be simplified to 2 sites (instead of 4).

2.3. Mean-field approximations for the paramagnetic Kondo phase

Here, we describe the mean-field impurity solver that we used in order to solve the local action (3) for the paramagnetic Kondo phase (K). We decoupled Kondo interaction by means of mean-field approximation as introduced by Lacroix and Cyrot in [11], which was shown to be analogous to the "large N" expansion or slave boson approximation developed by Coleman in [29] and Read and Newns in [30]. In numerous occasions (see, e.g., [11,5,31–37]) this approximation was proven to be efficient for describing the low energy properties of the Kondo lattice.

At first, we represent spin operators within Abrikosov's fermionic representation $\mathbf{S}_\alpha^{\sigma\sigma'} = f_{\alpha\sigma}^\dagger f_{\alpha\sigma'} - \delta_{\sigma\sigma'}/2$ thereafter the Kondo interaction is mapped as $\mathbf{S}_\alpha \mathbf{s}_\alpha \rightarrow \frac{1}{2} \sum_{\sigma\sigma'} c_{K\alpha\sigma}^\dagger c_{K\alpha\sigma'} f_{K\alpha\sigma}^\dagger f_{K\alpha\sigma'}$. Then the Kondo interaction is decoupled using mean-field as $\mathbf{S}_\alpha \mathbf{s}_\alpha \approx -\frac{1}{2} \sum_{\sigma\sigma'} \langle c_{K\alpha\sigma}^\dagger f_{K\alpha\sigma} \rangle f_{K\alpha\sigma'}^\dagger c_{K\alpha\sigma'} + \langle f_{K\alpha\sigma'}^\dagger c_{K\alpha\sigma'} \rangle c_{K\alpha\sigma}^\dagger f_{K\alpha\sigma} - \langle f_{K\alpha\sigma'}^\dagger c_{K\alpha\sigma'} \rangle$. An

effective Kondo c-f hybridization appears due to the decoupling, defined as $r_\alpha = \frac{J_K}{2} \sum_{\sigma} \langle c_{K\alpha\sigma}^\dagger f_{K\alpha\sigma} \rangle$. Additional local constraint $\sum_{\sigma} f_{K\alpha\sigma}^\dagger f_{K\alpha\sigma} = 1$ should be added to restrict the number of Abrikosov's fermions to one per site which is imposed by introducing a Lagrange parameter λ_α . As done in most cases, this constraint is considered only in average on the lattice and this Lagrange multiplier is identified to an effective energy level for the auxiliary f fermions.

Since here we are treating pure Kondo phase with all A-sites equivalent to B-sites, the mean-field parameters r_α and λ_α becomes site independent as long as α site is a Kondo site. Therefore, we skip the α and σ indices. Then the expressions for local Green function $G_K^c(\tau)$ are obtained as

$$G_K^c \left(i\omega \right) = \frac{1}{i\omega + \mu - \Delta(i\omega) - \frac{r^2}{i\omega + \lambda}}, \quad (5)$$

$$G_K^{cf} \left(i\omega \right) = \frac{-r}{(i\omega + \mu - \Delta(i\omega))(i\omega + \lambda) - r^2}, \quad (6)$$

$$G_K^f \left(i\omega \right) = \frac{1}{i\omega + \lambda - \frac{r^2}{(i\omega + \mu - \Delta(i\omega))}}. \quad (7)$$

For a non-Kondo site, the Green function can be obtained directly from the electronic bath Δ :

$$G_N^c = \frac{1}{i\omega + \mu - \Delta(i\omega)}. \quad (8)$$

The chemical potential μ , the effective energy level λ and the effective hybridization r are determined by solving the following self-consistent equations

$$n_c = x \frac{2}{\beta} \sum_{i\omega} G_K^c \left(i\omega \right) + \left(1 - x \right) \frac{2}{\beta} \sum_{i\omega} G_N^c \left(i\omega \right), \quad (9)$$

$$r = J_K \frac{1}{\beta} \sum_{i\omega} G_K^{cf} \left(i\omega \right), \quad (10)$$

$$1 = \frac{2}{\beta} \sum_{i\omega} G_K^f \left(i\omega \right). \quad (11)$$

In this mean-field description, r is an order parameter for the Kondo paramagnetic phase. It describes the low temperature magnetic entanglement between conduction electrons and Kondo impurities spins. The Kondo crossover temperature is replaced by a transition at Kondo temperature T_K , defined as the temperature where r continuously vanishes. It can be computed from J_K by solving the equation $\frac{1}{J_K} = -\frac{1}{\beta} \sum_{i\omega} \frac{G_0(i\omega)}{i\omega}$, where $G_0(i\omega)$ is the non-interacting Green's function and is independent on x , as discussed in [25].

The Eqs. (9)–(11) together with (5)–(8) are solved self-consistently to find the self-consistent solutions for μ , λ and r and $\Delta(i\omega)$.

2.4. Mean-field approximations for ferromagnetic (F) and antiferromagnetic (AF) phases

We restrict our study of Kondo alloys to pure ordered phases, and we ignore the possibility of mixed phases where Kondo effect and magnetic order would co-exist. Following the symmetries allowed by F and AF phases (see Table 1), we restrict our study on the sub-lattice A for both spins \uparrow and \downarrow . Consequently, hereafter, in this section we consider only $\alpha = A$ and we omit the α index. The Kondo interaction is decoupled using Weiss mean-field channel as $\mathbf{S} \mathbf{s} \approx \langle S^z \rangle s^z + S^z \langle s^z \rangle - \langle S^z \rangle \langle s^z \rangle$, and the order parameters are the local magnetizations of impurity spins and c-electrons on a site A

$$\langle S^z \rangle = m_f = \frac{1}{2} \sum_{\sigma} \sigma_z \left\langle f_{K\sigma}^\dagger f_{K\sigma} \right\rangle, \quad (12)$$

$$\langle s^z \rangle = m_c = \frac{1}{2} \sum_{\sigma} \sigma_z \left\langle c_{\sigma}^\dagger c_{\sigma} \right\rangle. \quad (13)$$

The local effective problem described by the action (3) can be solved explicitly. We obtain the expression for local Green function $G_K^c(\tau)$ of the magnetic ordered phases for K -sites as

$$G_K^c \sigma = \frac{1}{i\omega + \mu - \Delta_\sigma(i\omega) - \sigma_z J_K \frac{m_f}{2}}, \quad (14)$$

and for N -sites as

$$G_N^c \sigma = \frac{1}{i\omega + \mu - \Delta_\sigma(i\omega)}. \quad (15)$$

The chemical potential μ and the order parameters m_f^z and m_c^z are

determined by solving the self-consistent equations

$$n_c = x \frac{1}{\beta} \sum_{i\omega, \sigma} G_{K\sigma}^c(i\omega) + \left(1 - x\right) \frac{1}{\beta} \sum_{i\omega, \sigma} G_{N\sigma}^c(i\omega), \quad (16)$$

$$m_c = \frac{1}{2\beta} \sum_{i\omega, \sigma} \sigma_z G_{K\sigma}^{cc}(i\omega), \quad (17)$$

$$m_f = -\frac{1}{2} \tanh\left(\frac{\beta m_c J_K}{2}\right). \quad (18)$$

These Eqs. (16)–(18) together with (14), (15) are solved self-consistently using the DMFT/CPA in order to find the self-consistent solutions for μ , m_f and m_c . The results are presented in the next section.

3. Results

In this section, we present and discuss the ground state phase diagrams obtained for periodic Kondo lattice and for Kondo alloys for $n_c = 0.30$ and 0.90 . In each case, the phase diagrams were obtained by comparing the energies of each phase considered after subtracting energy of the system without interaction ($J_K = 0$). At first, we studied the phase diagrams for periodic Kondo lattice for 1D ‘chain’, 2D ‘square’ and 3D ‘cubic’ lattices and we reproduced the existing results which validated our method. Then, we present the results for Kondo alloys.

3.1. Periodic Kondo lattice ($x = 1$) at $T = 0$

In order to validate our DMFT/CPA approach, we calculated the solutions for paramagnetic Kondo phase (K), for ferromagnetic phase (F), and for commensurate antiferromagnetic phases for periodic 1D ‘chain’, 2D ‘square’ and 3D ‘cubic’ Kondo lattices without using DMFT/CPA algorithm. We then studied the same problem for the 2D ‘square’ lattice using DMFT algorithm. For each case, we came up with same results obtaining the same phase diagram at $x = 1$.

Fig. 2 shows the phase diagrams obtained for 1D ‘chain’, 2D ‘square’ and 3D ‘cubic’ lattices at $T = 0$ with K, F and AF phases with several commensurate antiferromagnetic phases (cf. Table 2). The ground state phase diagrams are consistent with Doniach Phase diagram [10]. At small coupling (J_K), magnetically ordered (MO) phases are obtained while paramagnetic Kondo (K) dominates at larger J_K . One can easily notice that at small J_K , a cascade of antiferromagnetic phases to ferromagnetic phases is observed as we move from higher electronic filling (n_c) to lower electronic fillings (n_c) for each lattices. Since all three phase diagrams have the same form, we will concentrate on the 2D square lattice for the study of Kondo alloys.

3.2. Kondo alloy

We used the DMFT algorithm to study binary Kondo alloys for $x \in [0.01, 1]$ for different n_c and for different couplings J_K considering pure K, F and AFII phases.

We present below (Fig. 3) the ground state phase diagrams obtained for $n_c = 0.30$ and 0.90 . Here, the strength of the Kondo interaction is represented by the ratio between the corresponding Kondo temperature T_K and the non-interacting electronic bandwidth W .

We also determined the phase diagrams for other values of electronic filling (not presented here). All phase diagrams have a lot of similarities, and are Doniach-like: at low Kondo temperature (T_K) MO phase is found to be the ground state and this MO phase is suppressed by the paramagnetic Kondo phase at higher T_K . The persistence of MO down to very low impurity concentrations is remarkable. This could be explained by the long range of the RKKY interaction.

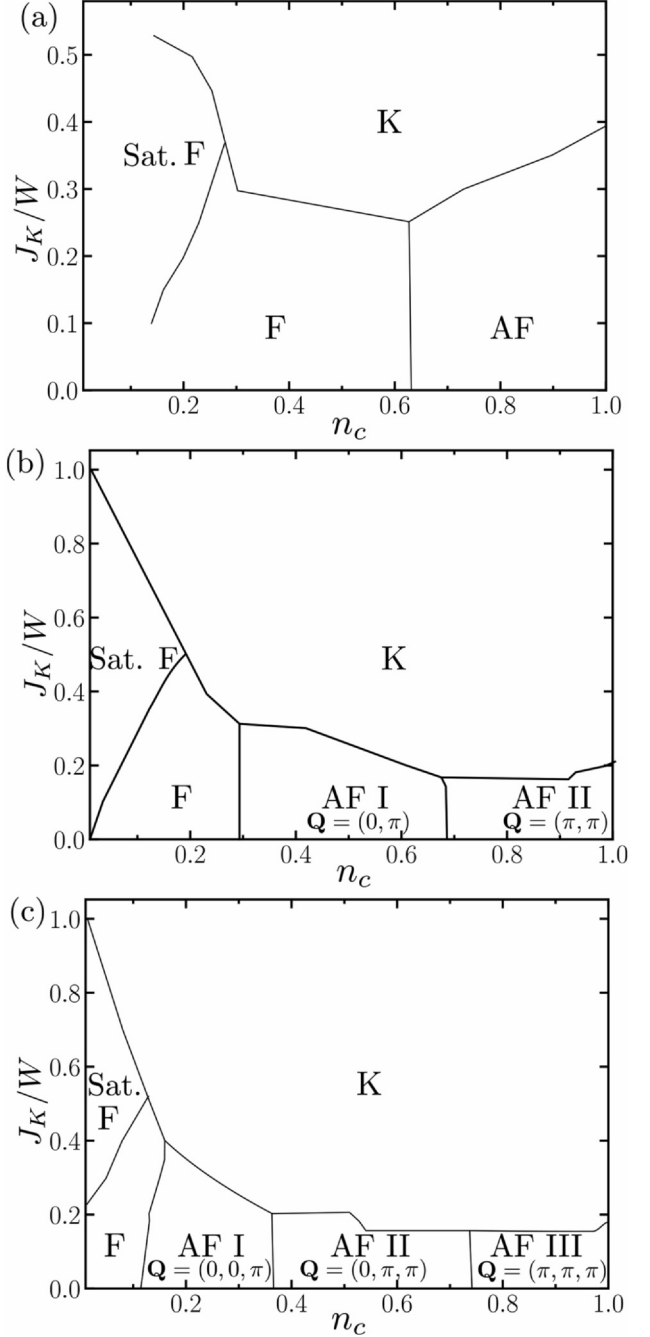


Fig. 2. phase diagrams (a) 1D ‘chain’, (b) 2D ‘square’, (c) 3D ‘cubic’ lattices at $T = 0$. K = paramagnetic Kondo phase, F = ferromagnetic phase (conduction electrons partly polarized), sat. F = saturated ferromagnetic phase (conduction electrons fully polarized) and AF = antiferromagnetic phase. W denotes the non-interacting electronic bandwidth.

Table 2

Commensurate AF phases considered here, with their respective ordering wave vectors.

	\mathbf{Q}_0^{AFI}	\mathbf{Q}_0^{AFII}	\mathbf{Q}_0^{AFIII}
1D	π		
2D	$(\pi, 0)$	(π, π)	
3D	$(0, 0, \pi)$	$(\pi, \pi, 0)$	(π, π, π)

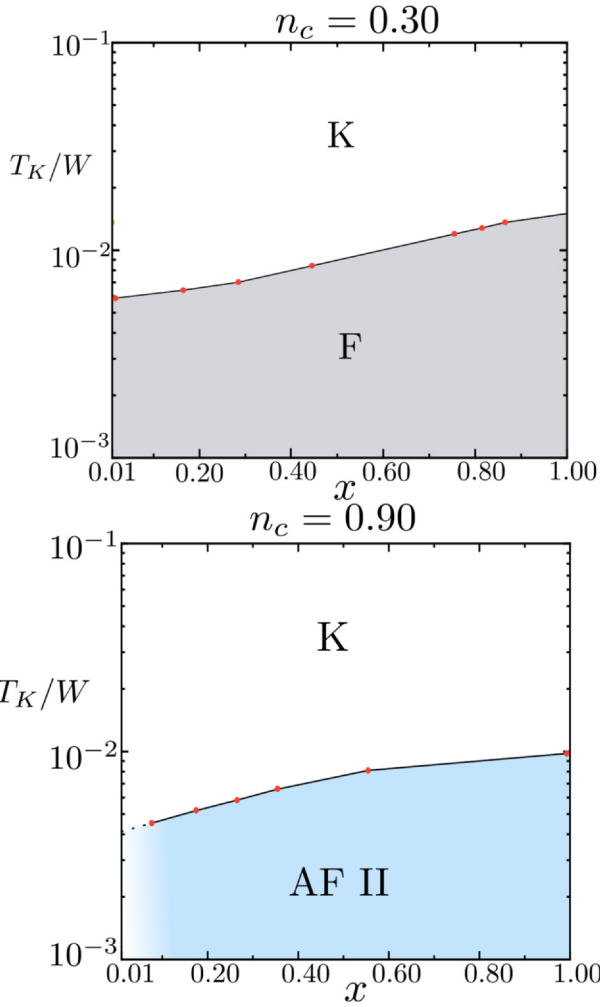


Fig. 3. Ground state phase diagrams of the Kondo alloys on a square lattice for $n_c = 0.30$ and 0.90 , with Kondo (K), Néel ordered anti-ferromagnetic (AF II), and ferromagnetic (F) phases.

4. Comparison with the experimental data with few Ce-based 122-family heavy fermion (HF) materials

In real isostructural Ce-La substitution series, experiments show that the strength of the Kondo interaction decreases when decreasing Cerium concentration. This is due to the effective pressure effect. In order to provide a scenario for real Kondo alloys, using the $(x-T_K)$ phase diagrams depicted on Fig. 3, Ce-La substitution can thus be characterized with a non-constant but rather monotonous variation of T_K as a function of x .

The Kondo versus magnetic order phase diagrams suggest a coherent scenario for Ce-La substitution in various HF materials. Here, we focus only on 122-family but the scenario isn't restricted to these compounds and we expect that it can be much more general. Fig. 4 is the generalized phase diagram obtained through DMFT/CPA calculations where we placed few Ce-based 122-family HF materials. For several of Kondo lattice ($x = 1$) 122 compounds, the Doniach argument is consistent with occurrence of magnetic ordered ground state when the strength of the Kondo coupling T_K becomes smaller than about 10 Kelvin. We can thus depict various Kondo alloys on a single schematic phase diagram, where the energy scale is arbitrarily fixed (see Fig. 4). For $\text{Ce}_x\text{La}_{1-x}\text{Pt}_2\text{Si}_2$, the paramagnetic phase persists with substitution, with T_K decreasing from 70 K ($x = 1$) to 2.6 ± 0.6 K ($x = 0.10$) [24]. For $\text{Ce}_x\text{La}_{1-x}\text{Ni}_2\text{Ge}_2$, the ground state also remains paramagnetic but the Kondo interaction is smaller, from 30 K for $x = 1$ to 1 K for $x = 0.01$

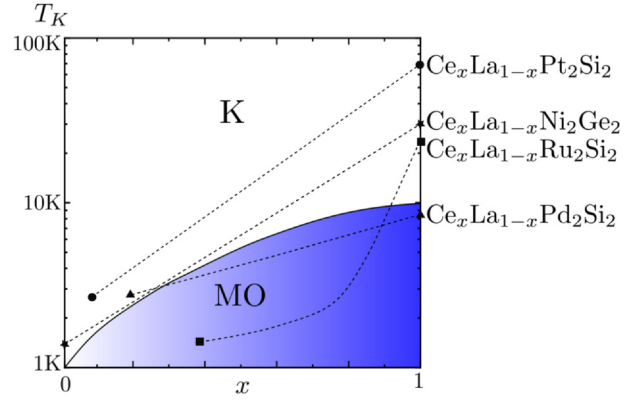


Fig. 4. Schematic description of the Kondo alloys phase diagrams depicted on Fig. 3, with Kondo (K) and magnetically ordered (MO) phases. In order to fix the energy scale, the K-MO transition is arbitrarily chosen to be realized here at $T_K \approx 10$ Kelvin for the Kondo lattice ($x = 1$) and at around 1 Kelvin in the dilute limit $x \ll 1$. Dashed lines describe four examples of Kondo alloys: $\text{Ce}_x\text{La}_{1-x}\text{Pt}_2\text{Si}_2$ (circle), $\text{Ce}_x\text{La}_{1-x}\text{Ni}_2\text{Ge}_2$ (star), $\text{Ce}_x\text{La}_{1-x}\text{Ru}_2\text{Si}_2$ (square) and $\text{Ce}_x\text{La}_{1-x}\text{Pd}_2\text{Si}_2$ (triangle).

[22]. Invoking the present scenario, the vicinity of a magnetically ordered phase at intermediate Ce concentration might explain the non-Fermi liquid behavior that has been reported for this Kondo alloy [22]. For $\text{Ce}_x\text{La}_{1-x}\text{Ru}_2\text{Si}_2$, the Kondo lattice ($x = 1$) is paramagnetic with $T_K = 24$ K, but an antiferromagnetic ground state is stabilized below the critical concentration $x = 0.91$ [21] and down to the smallest concentrations for which this alloy was synthesized. The Kondo lattice CePd_2Si_2 , which is characterized by a smaller $T_K = 9$ K, has an antiferromagnetic ground state with a Néel temperature $T_N = 9.9$ K. For $\text{Ce}_x\text{La}_{1-x}\text{Pd}_2\text{Si}_2$, the antiferromagnetic phase is observed when $x > 0.75$, but a paramagnetic Kondo ground state is obtained at lower Cerium concentrations, with T_K decreasing down to 2.8 K for $x = 0.20$ [38]. Another example of 122 Ce-La substituted compound has a similar behaviour as CePd_2Si_2 : the Kondo alloy $\text{Ce}_x\text{La}_{1-x}\text{Cu}_2\text{Ge}_2$ was indeed reported to be antiferromagnetic with $T_N = 4.1$ K and $T_K = 4$ K for $x = 1$, and a surprising persistence of antiferromagnetic order down to $x = 0.10$ [23]. Our present scenario might also explain this persistence. Of course, the quantitative energy scale used for the schematic Fig. 4 was chosen arbitrarily in order to mimic various 122 Ce-based compounds in a coherent scenario. However, we expect that the qualitative properties observed experimentally should remain universal beyond the specific cases that are analyzed here.

5. Conclusion

Using the DMFT/CPA method together with standard mean-field approximations, we have extended the Doniach phase diagram to Kondo alloys where Kondo ions can be substituted with non-Kondo ones. We find that the long range magnetic order which is predicted at small Kondo coupling can be persistent down to very low concentration of Kondo spins. This persistence is related with the long range nature of the RKKY interaction. Our results provide a coherent scenario for Ce-La substitution in several compounds. It is illustrated here by a few examples from the 122 family, $\text{Ce}_x\text{La}_{1-x}\text{Pt}_2\text{Si}_2$, $\text{Ce}_x\text{La}_{1-x}\text{Ni}_2\text{Ge}_2$, $\text{Ce}_x\text{La}_{1-x}\text{Ru}_2\text{Si}_2$, $\text{Ce}_x\text{La}_{1-x}\text{Pd}_2\text{Si}_2$, and $\text{Ce}_x\text{La}_{1-x}\text{Cu}_2\text{Ge}_2$, that exhibit absence of magnetic order, non-Fermi liquid behavior, persistence of magnetic order, or reentrance magnetic order upon Cerium dilution. Beyond the 122 family and the Cerium-based compounds, this scenario should be relevant for most of other Kondo alloys. The issue of a possible breakdown of coherence and Fermi surface reconstruction that might characterize the paramagnetic phase was not analyzed here and it will be investigated in further works.

References

- [1] A.C. Hewson, *The Kondo problem to heavy fermions vol. 2*, Cambridge University Press, 1997.
- [2] P. Fulde, P. Thalmeier, G. Zwicknagl, Strongly correlated electrons, in: Henry Ehrenreich, Frans Spaepen (Eds.), *Solid State Physics*, Academic Press, vol. 6, 2006, p. 1.
- [3] P. Coleman, *Introduction to Many-Body Physics*, Cambridge University Press, Cambridge.
- [4] Y. Onuki, *Physics of Heavy Fermions*, World Scientific Publishing Company.
- [5] E. Pavarini, P. Coleman, E. Koch, *Many-Body Physics: From Kondo to Hubbard*, Tech. Rep., Theoretische Nanoelektronik, 2015.
- [6] C. Pfleiderer, Superconducting phases of f -electron compounds, *Rev. Mod. Phys.* 81 (2009) 1551–1624.
- [7] P. Thalmeier, G. Zwicknagl, Unconventional superconductivity and magnetism in lanthanide and actinide intermetallic compounds, *Handbook on the physics and chemistry of rare earths* 34 (2004) 135.
- [8] F. Steglich, J. Aarts, C.D. Bredl, W. Lieke, D. Meschede, W. Franz, H. Schäfer, Superconductivity in the Presence of Strong Pauli Paramagnetism: CeCu_2Si_2 , *Phys. Rev. Lett.* 43 (1979) 1892–1896.
- [9] H.v. Löhneysen, T. Pietrus, G. Portisch, H. Schlager, A. Schröder, M. Sieck, T. Trappmann, Non-Fermi-liquid behavior in a heavy-fermion alloy at a magnetic instability, *Phys. Rev. Lett.* 72 (20) (1994) 3262.
- [10] S. Doniach, The Kondo lattice and weak antiferromagnetism, *physica B+C* 91 (1977) 231–234.
- [11] C. Lacroix, M. Cyrot, Phase diagram of the Kondo lattice, *Phys. Rev. B* 20 (5) (1979) 1969.
- [12] P. Fazekas, E. Müller-Hartmann, Magnetic and non-magnetic ground states of the Kondo lattice, *Z. Phys. B Condens. Mat.* 85 (2) (1991) 285–300.
- [13] F. Assaad, Quantum Monte Carlo simulations of the half-filled two-dimensional Kondo lattice model, *Phys. Rev. Lett.* 83 (4) (1999) 796.
- [14] R. Peters, T. Pruschke, Magnetic phases in the correlated Kondo-lattice model, *Phys. Rev. B* 76 (24) (2007) 245101.
- [15] P. Nozières, Some comments on Kondo lattices and the Mott transition, *Eur. Phys. J. B-Condens. Mat. Complex Syst.* 6 (4) (1998) 447–457.
- [16] C. Lacroix, Coherence effects in the Kondo lattice, *J. Magn. Magn. Mater.* 60 (2–3) (1986) 145–152.
- [17] S. Burdin, A. Georges, D.R. Grempel, Coherence scale of the Kondo lattice, *Phys. Rev. Lett.* 85 (2000) 1048–1051.
- [18] B. Coqblin, C. Lacroix, M.A. Gusmão, J.R. Iglesias, Band-filling effects on Kondo lattice properties, *Phys. Rev. B* 67 (2003) 064417.
- [19] T. Pruschke, R. Bulla, M. Jarrell, Low-energy scale of the periodic Anderson model, *Phys. Rev. B* 61 (2000) 12799–12809.
- [20] A.N. Tahvildar-Zadeh, M. Jarrell, T. Pruschke, J.K. Freericks, Evidence for exhaustion in the conductivity of the infinite-dimensional periodic Anderson model, *Phys. Rev. B* 60 (1999) 10782–10787.
- [21] H. Aoki, N. Kimura, T. Terashima, Fermi surface properties, metamagnetic transition and quantum phase transition of CeRu_2Si_2 and its alloys probed by the dHvA effect, *J. Phys. Soc. Jpn.* 83 (7) (2014) 072001.
- [22] A.P. Pikul, U. Stockert, A. Steppke, T. Cichorek, S. Hartmann, N. Caroca-Canales, N. Oeschler, M. Brando, C. Geibel, F. Steglich, Single-ion Kondo scaling of the coherent Fermi liquid regime in $\text{Ce}_{1-x}\text{La}_x\text{Ni}_2\text{Ge}_2$, *Phys. Rev. Lett.* 108 (6) (2012) 066405.
- [23] H. Hodovanets, S.L. Bud'ko, W.E. Straszheim, V. Taufour, E.D. Mun, H. Kim, R. Flint, P.C. Canfield, Remarkably robust and correlated coherence and antiferromagnetism in $(\text{Ce}_{1-x}\text{La}_x)\text{Cu}_2\text{Ge}_2$, *Phys. Rev. Lett.* 114 (2015) 236601.
- [24] F. Ragel, P.d.V. du Plessis, A. Strydom, Effects of La dilution on the CePt_2Si_2 Kondo lattice, *J. Phys.: Condens. Matter* 20 (5) (2008) 055218.
- [25] S. Burdin, P. Fulde, Random Kondo alloys investigated with the coherent potential approximation, *Phys. Rev. B* 76 (2007) 104425.
- [26] W. Zu, Z.-Z. Li, The slave boson mean-field theory of two-conduction-band Kondo alloys, *J. Phys. C: Solid State Phys.* 21 (22) (1988) 4083.
- [27] S. Burdin, C. Lacroix, Breakdown of coherence in Kondo alloys: crucial role of concentration vs band filling, *J. Phys.: Condens. Matter*.
- [28] A. Georges, G. Kotliar, W. Krauth, M.J. Rozenberg, Dynamical mean-field theory of strongly correlated fermion systems and the limit of infinite dimensions, *Rev. Mod. Phys.* 68 (1) (1996) 13.
- [29] P. Coleman, $\frac{1}{N}$ expansion for the Kondo lattice, *Phys. Rev. B* 28 (9) (1983) 5255.
- [30] N. Read, D. Newns, S. Doniach, Stability of the Kondo lattice in the large- N limit, *Phys. Rev. B* 30 (7) (1984) 3841.
- [31] B. Bernhard, B. Coqblin, C. Lacroix, Frustration in the Kondo lattice model: local versus extended singlet phases, *Phys. Rev. B* 83 (21) (2011) 214427.
- [32] B. Bernhard, C. Lacroix, Coexistence of magnetic order and Kondo effect in the Kondo-Heisenberg model, *Phys. Rev. B* 92 (9) (2015) 094401.
- [33] J.R. Iglesias, C. Lacroix, B. Coqblin, Revisited Doniach diagram: Influence of short-range antiferromagnetic correlations in the Kondo lattice, *Phys. Rev. B* 56 (18) (1997) 11820.
- [34] N. Perkins, J. Iglesias, M. Núñez-Regueiro, B. Coqblin, Coexistence of ferromagnetism and Kondo effect in the underscreened Kondo lattice, *EPL (Europhysics Letters)* 79 (5) (2007) 57006.
- [35] P. Coleman, N. Andrei, Kondo-stabilised spin liquids and heavy fermion superconductivity, *J. Phys.: Condens. Mat.* 1 (26) (1989) 4057.
- [36] Y. Liu, G.-M. Zhang, L. Yu, Weak ferromagnetism with the Kondo screening effect in the Kondo lattice systems, *Phys. Rev. B* 87 (13) (2013) 134409.
- [37] A. Hackl, M. Vojta, Kondo volume collapse, Kondo breakdown, and Fermi surface transitions in heavy-fermion metals, *Phys. Rev. B* 77 (13) (2008) 134439.
- [38] M. Besnus, A. Braghta, A. Meyer, Kondo behaviour in magnetic $(\text{Ce-La})\text{Pd}_2\text{Si}_2$, *Z. Phys. B Condens. Mat.* 83 (2) (1991) 207–211.